JOURNAL OF CATALYSIS 98, 457–467 (1986)

Pore Size Effects on Sintering of Ni/Al_2O_3 Catalysts

JAMES T. RICHARDSON AND JAMES L. PROPP

Department of Chemical Engineering, University of Houston, University Park, Houston, Texas 77004

Received January 10, 1985; revised October 3, 1985

Effects of pore size on sintering kinetics of Ni/Al_2O_3 catalysts have been studied with *in situ* magnetization and hydrogen chemisorption measurements. Three samples of γ-Al_2O_3 were prepared differing only in pore size distributions, with average pore radii of 4.1, 5.4, and 7.6 nm, respectively. These samples were loaded with 7 wt% nickel using homogeneous deposition. Nickel crystallite size distributions were very narrow at 2- to 2.3-nm radius. Sintering in helium at 500 and 600°C increased crystallite size but decreased accessibility of the nickel surface, due to physical blockage and not electronic effects. Measurements before and after loading showed only small changes in pore size distribution. Initial sintering rates increased by a factor of 4 as pore size doubled. Nickel surface areas followed the decay curve $dS/dt = -kS^n$ with k increasing by about a factor of 1000 while n remained in the range 7–10. Crystallite size distributions were stable after 20 h but surface blockage occurred for crystallites approaching the pore radii in size with sintering confined to individual pores.

INTRODUCTION

Metal catalysts are generally used in the form of small metal crystallites dispersed on high-surface-area supports. Small crystallites have large surface energies and grow to minimize this energy. Agglomeration, or sintering, occurs at high temperatures and reduces metal surface area, thereby decreasing the catalytic activity. Sintering also changes the crystallite size distribution, affecting both activity and selectivity (*2*).

Two predominant sintering models have evolved in recent years: interparticle transport and crystallite migration (*2*). Interparticle transport, frequently called atomic migration, involves escape of metal atoms from the crystallite to the support or into the gas phase and subsequent migration and capture by larger crystallites. Crystallite migration is movement of crystallites over the support, followed by collision and coalescence. This model is analogous to a two-dimensional random walk.

Interparticle transport of metal atoms may be equated to evaporation and condensation processes of liquid droplets of different sizes. This model was developed by Flynn and Wanke (*3–6*). Similar to transport of material from smaller to larger droplets due to variations in equilibrium vapor pressure with radius, smaller crystallites equilibrate with larger atomic concentrations. Small crystallites loose atoms while larger crystallites grow. Localized metal–support interactions, due to the presence of metal oxide or support surface defects (*7*), reduce the energy differences between an atom in a crystallite and on the surface to values where atoms escape from crystallites to the support surface (*5*). Several authors report considerable mobility for atoms on supports, even at temperatures below those normally encountered in catalyst sintering (*7*). The rate at which crystallites gain atoms depends on surface concentration, atomic diffusivity, and crystallite diameter. Surface loading is very significant since it determines the surface concentration of migrating atoms and thus the capture rate. High loadings sinter faster. For rapid capture, this model predicts a monotonically decreasing metal dispersion. However, for slow capture, dispersion increases and then decreases. Redispersion

0021-9517/86 $3.00

can occur due to trapping of metal atoms at high-energy sites on the support surface or termination of migration with rapid cooling (*8*).

This interparticle transport model predicts growth of large crystallites and an increase in the number of small crystallites. Therefore, the initial crystallite size distribution broadens as crystallites smaller than the initial minimum size are generated. The model also predicts a final distribution strongly dependent on initial distribution. Broad or multimodal distributions sinter more rapidly than narrow distributions. Furthermore, a unisized distribution should not sinter. The model also predicts redispersion if the capture rate is slow.

Two mechanisms for atomic migration have been suggested (*2*). The first involves a two-dimensional phase of single atoms dispersed over the substrate and serving as an intermediate between small and large crystallites. The second, discussed by Ruckenstein and Dadyburjes and called direct ripening, invokes direct transport from small to large crystallites (*9*).

The model for binary collision between migrating crystallites was developed by Ruckenstein and Pulvermacher (*10–12*). Crystallites diffuse across the support surface, collide with other crystallites, and coalesce. Crystallite motion is slow compared to coalescence at sintering temperatures and diffusion controls sintering rate. A universal distribution, independent of initial distribution, results on homogeneous surfaces. Nonhomogeneous surfaces give equilibrium crystallite size distributions after sufficiently long sintering times. This model predicts rapid sintering of catalysts with unisized or narrow crystallite size distributions.

Wynblatt and Gjostein (*13*) postulated that both sintering mechanisms contribute to surface loss. The relative importance of each mechanism depends on the average size of the crystallites. Since only crystallites smaller than about 5 nm radius are mobile, crystallite migration dominates for these small crystallites while large crystallites grow primarily by interparticle transport.

Granquist and Buhrman (*14–17*) concluded that interparticle transport and crystallite migration lead to different crystallite size distributions. These differences identify the mechanism. Interparticle transport predicts "a tail" on the low-radius side of the distribution and crystallite migration on the high-radius side. However, Wanke (*18*) states that a lognormal shape distribution via interparticle transport is also obtained by sintering certain initial crystallite distributions. Initial changes in the crystallite distribution provide the most information. Crystallite migration leads to an increase in the average crystallite size with the disappearance of small crystallites. However, interparticle transport predicts an initial broadening of the distribution as small crystallites are generated, followed by increases in size at later times. This method of mechanism discrimination must be modified if crystallite splitting occurs (*13*). Crystallite migration also predicts sintering rates relatively insensitive to initial distribution, while interparticle transport indicates a certain dependence. If large metal–support interactions exist, atomic migration gives high sintering rates due to accelerated migration along the support. However, crystallite migration predicts low sintering rates due to small mobility of metal crystallites.

Both models lead to a sintering rate equation

$$\frac{dS}{dt} = -k \cdot S^n, \qquad (1)$$

where S is the metallic surface area. The rate constant, k, obeys the Arrhenius law and depends upon an activation energy and the sintering temperature (*3*). Exponent values reported in the literature range from 1 to 13 (*6*) and Wynblatt and Gjostein (*13, 21*) found time dependence.

The exponent n of the power-law sintering expression has been used to differenti-

ate the two mechanisms (*6*). An exponent less than or equal to 3 signifies interparticle transport while a value greater than 3 indicates crystallite migration. However, Wynblatt and Ahn (*19*) suggested that faceted crystallites exhibit a retarding effect on sintering. This concept explains large exponent values in apparent interparticle transport cases, but implies that assignment of the mechanism solely on the basis of exponent values is not feasible. Furthermore Desai and Richardson (*20*) documented that measured surface areas do not necessarily reflect crystallite size since inaccessibility due to surface interactions or pore trapping may occur.

Lee recently developed a modification of the theory for atomic migration leading to (*21*)

$$\frac{dS}{dt} = -k \cdot S^n \exp(ms). \qquad (2)$$

Equation (2) fits available data as well as Eq. (1) with n values from 3 to 5 and m a function of metal loading, temperature, and support properties.

Least understood is the role of the support on sintering. Wynblatt and Ahn (*19*) suggested that pore and surface structures affect sintering rates. These include metal–support interactions and pore effects. Pask and Fulrath (*22*) postulated incorporation of metal atoms into the support structure in the presence of oxygen. Geus (*7*) reported that oxygen significantly increased interaction of metal crystals and oxide supports. Geus also observed an increase in metal–support interactions when impurities exist in the support surface. Bartholomew and co-workers compared the sintering rates of nickel on silica and alumina in the presence of H_2 and H_2O (*23, 24*).

Pores of the support also influence the sintering rate. Collapse of pore structure at high temperatures increases the sintering rate. Williams *et al.* (*25*) reported nickel area loss directly related to coalescence of nickel crystallites following decrease in support surface. Wynblatt and Gjostein (*13*) postulated that concavities in the support surface stabilize metal particles whose dimensions and volumes are commensurate with those of the support. Some metal particles become trapped in the pores. Kuo *et al.* (*26*) suggested that pore size distribution has an influence on sintering mechanisms.

A theoretical model was advanced by Ruckenstein and Pulvermacher who considered sintering of crystallites in unisized pores via the migration mechanism (*27*). Sintering rates were predicted to vary inversely with surface area when crystallite radii were smaller than those of the pores. The decay parameter, n, decreases to values as low as 3 when radii ratios exceed 0.5. Crystallite distributions achieve a steady state after long times.

This paper reports experimental effects of the pore size distribution on sintering rates of nickel–alumina catalysts. Nickel catalysts are used industrially in hydrogenation, hydrotreating, and steam reforming processes. New applications of these catalysts were developed for methanation of coal-derived synthesis gas (*28, 29*). Alumina was selected as the support since the pore structure is easily varied. Nickel exhibits superparamagnetic properties from which crystallite size distributions can be calculated (*30*) and is a good candidate for these studies. In addition, Richardson and co-workers (*31, 32*) made extensive studies on sintering of Ni/SiO_2 catalysts, giving a comparison with other systems.

EXPERIMENTAL

Support selection and characterization. The objective was to study sintering kinetics on samples of Ni/Al_2O_3 differing only in pore size distributions of the support, i.e., nickel loadings, crystallite size distributions, support interactions, etc., must be similar. Accordingly, it was necessary to select an alumina with an average pore size in the same range as the expected crystallite size (1.5–3.0 nm radius). Different supports could then be generated before nickel depo-

sition by heat treatment of the initial material.

Supports were characterized by measurement of nitrogen adsorption and desorption isotherms at liquid-nitrogen temperature using a Micromeritics Surface-Area Pore-Volume Analyzer Model 2100 D. BET surface areas, *t*-plots, and pore size distributions were calculated using standard procedures (*33*). Pore size and shape analysis were carried out in the usual manner.

A number of commercial aluminas were examined and Alfa Products 87224 selected as the most appropriate. Table 1 gives the texture properties of this support.

The *t*-plots showed positive deviation, indicating capillary condensation in mesopores. Hysteresis loops were steep at intermediate relative pressure (Type A) implying cylindrical pores. Furthermore, the cumulative surface area calculated from the desorption branch, S_{DES}, is equivalent to the BET surface area, again indicating cylindrical shapes. The surface average pore size is 3.0 nm with 91% of the pores less than 3.6 nm in size.

Sintering temperature in the range 500 to 600°C were anticipated. Since it is necessary that the support remain unchanged during sintering, suitable samples were prepared by heat treatment of the Alfa Products 87224 above 600°C. A series of exploratory heat treatments was performed and the products characterized. Three samples were selected, as shown in Table 2.

TABLE 1

Characterization of Alfa Products 87224

S_{BET}	150 m²/g
S_{ADS}	139 m²/g
S_{DES}	151 m²/g
S_t	176 m²/g
R_p	3.0 nm
$S < 3.6$	91%

Note. S_{BET}, surface area from BET equation; S_{ADS}, surface area calculated from the pore size distribution determined from the adsorption branch; S_{DES}, surface area calculated from the pore size distribution determined from the desorption branch; S_t, *t*-plot surface area; $S < 3.6$ cumulative surface % less than 3.6 nm pore radius.

TABLE 2

Characterization of Supports

	Support		
	L	M	H
Temperature of heat treatment (°C)	600	800	950
Time of heat treatment (h)	18	24	27
S_{BET} (m²/g)	107	73.6	40.0
S_{ADS} (m²/g)	114	91.2	38.1
S_{DES} (m²/g)	124	93.9	48.0
S_t (m²/g)	134	74.8	43.8
R_p (nm)	4.1	5.4	7.6
$R < 0.1$ (nm)	1.9	2.7	2.9
$R < 0.9$ (nm)	8.1	14	20

The three samples, L, M, and H, consist of γ-Al_2O_3 heat-treated at 600, 800, and 950°C, respectively. Average pore radii increase from 4.1 to 7.6 nm with the distributions from 10 to 90% of the surface ($R < 0.1$ to $R < 0.9$) increasing accordingly. Hysteresis loops show cylindrical pores, although the lower S_{BET} values indicate some degree of pore constriction that increased with heat-treatment temperature. Higher temperatures than 950°C result in severe pore neck constriction and even ink-bottle pores. Supports L, M, and H are acceptable inasmuch as the only differences appear to be in the pore size distributions.

Nickel deposition. An initial narrow crystallite size distribution was desired. Since the pores are approximately the same size as the nickel crystallites, some pore entrapment (and subsequent lower nickel surface area) was expected. The homogeneous precipitation method of Van Dillen *et al.* (*34*) has been used extensively in this laboratory to produce small and narrow distributions (*35*). Very reproducible results have been obtained using silica as the support. Ac-

cordingly, the same method was adopted here. Since nickel forms larger crystallites when precipitated on alumina (*35*), smaller nickel loadings were used than before. Each alumina was slurried in deionized water after evacuation of the pores. Nickel nitrate and urea were added and the solution heated to 90°C. Urea slowly decomposed and nickel hydroxide precipitated on the alumina. After reacting for 1 h, the slurry was cooled, filtered, and washed. The catalyst cake was dried overnight at 120°C in an oven and sized with a 60-mesh screen.

Total amounts of nickel, determined with a variable absorbance method (*36*), are given in Table 3.

Magnetic and chemisorption measurements. Reduction and sintering of Ni/Al_2O_3 catalysts together with associated magnetic and hydrogen chemisorption measurements were carried out in the same *in situ* apparatus described by Cale and Richardson (*30*). Each sample was freshly loaded into the quartz cell and carried through a prescribed sequence of reduction and sintering steps. After each step, the catalyst was cleaned of adsorbed hydrogen by sweeping with purified helium (80 cm^3/min, 2 h, 375°C) and the cell transferred to the magnetometer for measurement of magnetization at 25 and −196°C. Nickel crystallites saturate magnetically at low temperature, giving the value of M_∞ necessary for further analysis of the distribution. This also gives the degree of reduction, an important parameter in both sintering and chemisorption interpretation. Magnetization versus magnetic field curves at 25°C were used to calculate nickel crystallite size distributions, using the same procedures reported by Cale and Richardson (*30*).

Following each magnetic characterization, the cell was connected to the hydrogen chemisorption apparatus (*30*) and the volumetric adsorption isotherm measured for pressures up to 300 Torr. Isotherms showed the characteristic shape of irreversible, rapid uptake followed by slow reversible adsorption, linear with pressure. Richardson and Cale have discussed in detail the significance of this isotherm (*37*). In accordance with their conclusions, the exposed surface of nickel was determined from the amount of irreversible adsorption, V_0, found by extrapolation of the expression

$$V_{ads} = V_0 + bP_H^{1/2}. \quad (1)$$

After chemisorption measurement, the cell was returned to the reduction-sintering apparatus for the next step in the sequence.

Catalyst reduction. Each catalyst was reduced under identical conditions: 80 cm^3 H_2/min, 1 h, at 250°C, 3 h at 350°C. Degree of reduction under these conditions ranged from about 60 to 70%. Initial distributions were very narrow with average (volume) radii, R_V, of about 2 nm.

Sintering conditions. All catalysts were sintered under the same conditions: 80 cm^3 He/min, 500°C for 1, 2, 5, and 20 h. A sample of M was also sintered at 600°C.

Texture of reduced and sintered catalyst. It is important that pore structure of the support does not change during the reduction and sintering process. A sample of each catalyst was reduced under identical conditions given above, cleaned in helium at 375°C, cooled in helium to room temperature, and passivated by flowing helium containing 2% oxygen. Richardson and Dubus demonstrated that this method effectively passivates the nickel surface without changing the crystallite size distributions (*35*). Properly protected, the samples were transferred to the nitrogen adsorption apparatus for measurement of S_{BET} and pore size distribution.

Also, samples sintered for 20 h were passivated after all other measurements were completed and given the standard texture analysis.

TABLE 3
Total Nickel Content

Support	Wt% Ni
L	7.0
M	6.8
H	6.8

Results given in Table 4 confirm that sintering does not change the texture of the samples. For the higher area supports, L and M, there is a slight increase in surface area. This is to be expected, since the dilute but highly dispersed nickel adds further surface. For the low surface sample, H, there is considerable decrease in area and the average pore size decreases. This is consistent with the observation that pores in this sample are more constricted. Crystallites block pore mouths, with a substantial decrease in area. As a test of this, the sintered samples were treated with dilute hydrochloric acid to dissolve the nickel. The value of S_{BET} increased from 26.8 to 40.0 m^2/g, the same as the original support, indicating that loss of surface area was indeed due to the presence of nickel crystallites, most likely blocking narrow constrictions.

RESULTS AND DISCUSSION

Typical magnetization curves are shown in Fig. 1 for the H support sintered at 500°C, designated as H-500. Crystallite size distributions for the three supports are given in Figs. 2, 3, and 4. All show similar initial distributions which increase through loss of small crystallites leading to larger average sizes. Although this behavior suggests crystallite migration, it is not by itself conclusive, neither are the distribution shapes definitive. Sintering of the M sample at 600°C, demonstrated in Fig. 5, shows the same effect but with more dramatic increase in the distribution.

TABLE 4

Pore Characteristics of Samples

Sample		Before loading support	After loading	
			Reduced	Sintered
L	S_{BET} (m^2/g)	107	111	105
	R_p (nm)	4.11	3.41	3.68
M	S_{BET} (m^2/g)	73.6	74.6	74.1
	R_p (nm)	5.41	4.65	5.22
H	S_{BET} (m^2/g)	40.0	29.9	26.8
	R_p (nm)	7.59	6.92	8.99

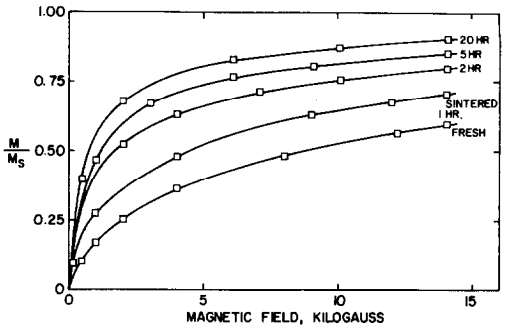

FIG. 1. Typical magnetization curves H-500, fresh and sintered.

It should be noted that the value of M_∞ for each sample remained constant within experimental error. This significant obser-

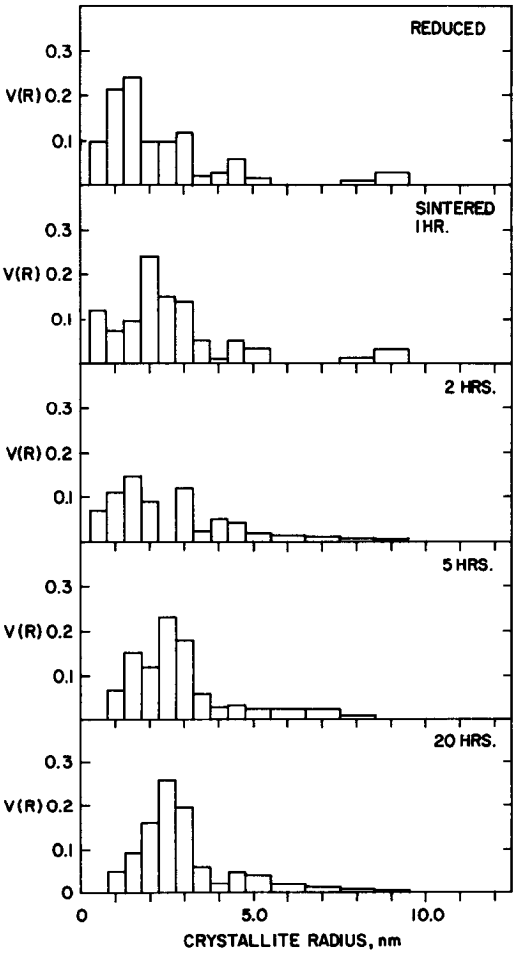

FIG. 2. Crystallite size distributions for sintering L-500.

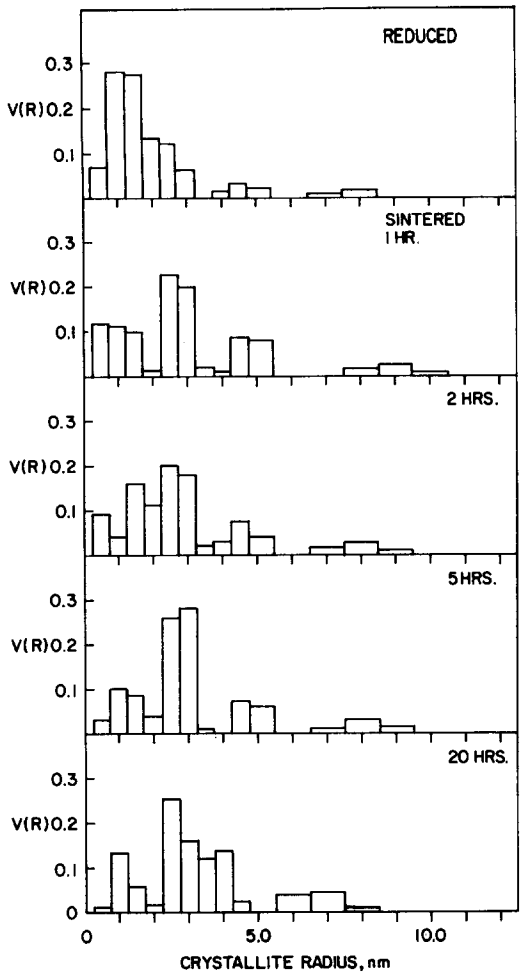

FIG. 3. Crystallite size distributions for sintering M-500.

vation indicates that no nickel was lost either by oxidation or combination with the support.

Nickel concentration was essentially identical for these samples and the degree of reduction the same. Another parameter that influences sintering rate is the number of crystallites per unit surface. This number, ϕ_0, may be calculated from the weight fraction of reduced nickel, the crystallite size distributions and the total surface area, S_{BET}. Table 5 gives the results for these samples and demonstrates that the numbers are approximately the same.

Differences in sintering kinetics can only be ascribed to the effect of pore size distribution since initial distribution, metal loading, crystallite concentration, and sintering conditions are the same. It has already been demonstrated that pore structure is invariant during sintering.

In order to quantify the sintering kinetics we adopt the procedure used previously by Richardson and Crump (*31*) and plot the calculated surface area, S_{calc}, against sintering time. This is shown in Fig. 6. It should be noted that this procedure assumes that the crystallites are spheres. The magnetic characterization gives a volume distribution and all resulting sizes are based on this assumption.

TABLE 5

Crystallite Surface Concentration

Sample	$\phi_0 \times 10^{-16}$ No. of crystallites/m^2
L-500	1.10
M-500	1.42
H-500	1.40
M-600	0.85

TABLE 6

Sintering Kinetic Parameters

Support	k	n
L-500	7.62×10^{15}	6.63
M-500	1.25×10^{19}	8.74
H-500	1.26×10^{19}	8.97
M-600	2.00×10^{21}	9.95

TABLE 7

Initial Rate of Surface Loss

Catalyst	Pore radius R_p (nm)	Crystallite radius,[a] $(R_V)_0$ (nm)	$-(dS/dt)_0$ (m^2/g · h)
L-500	4.11	2.25	32.6
M-500	5.41	1.94	67.1
H-500	7.59	1.95	137.3
M-600	5.41	1.97	245.1

[a] Initial volume average.

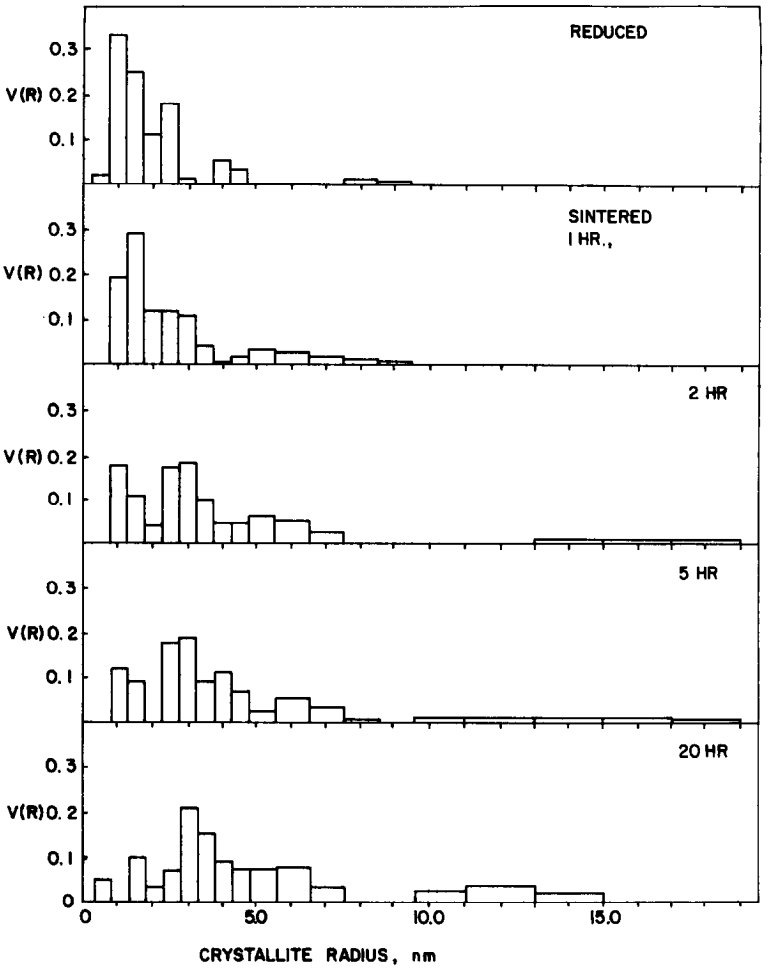

FIG. 4. Crystallite size distributions for sintering H-500.

Fitting Eq. (1) to the data in Fig. 6 gives the parameters in Table 6. Values of n from about 7 to 10 agree with previous results for crystallite migration in Ni/SiO_2 (*31*). Temperature dependence of the preexponential terms leads to an activation energy of 70 kcal/mol, similar to that found earlier for nickel on silica.

It is perhaps more informative to use not Eq. (1) but the initial rate of sintering as an index, as shown in Table 7. These data show that the initial sintering rate increases drastically as the pore size increases. This fact is consistent with the model of Ruckenstein and Pulvermacher which predicts a sintering rate inversely proportional to the surface area when crystallite radii are less than that of the pore and zero for greater sizes (*27*). The rates in Table 7 show a dependence of $(S_{BET})^{-0.7}$ but these pores are not unisized as assumed in the model. Furthermore, these authors indicate that n decreases as the ratio of the crystallite to pore radii increases, just as shown in Table 6. Steady-state crystallite distributions after long times are also indicated, again consistent with observations reported here. It is tempting to speculate that sintering occurs only in the domain of each individual pore and that the crystallites are stabilized after initial growth.

Pore structure also influences the final crystallite size distributions, which are almost stable. The H-500 catalyst has a very

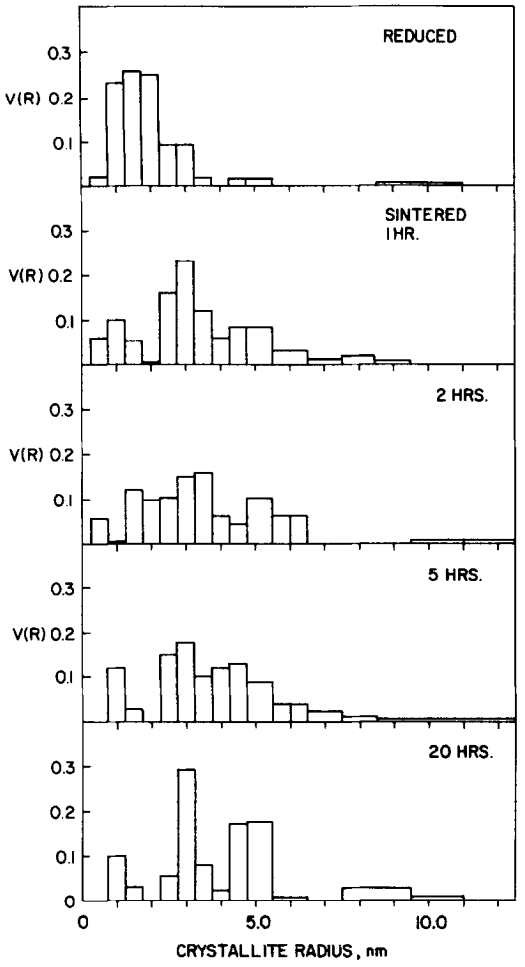

FIG. 5. Crystallite size distribution for sintering M-600.

TABLE 8

Measured Nickel Surface Areas

Sintering time (h)	Surface area, m^2/g			Ni
	L-500	M-500	H-500	M-600
0	58.0	107.7	81.7	101.1
1	40.7	68.0	56.3	37.8
2	25.9	55.4	37.2	26.3
5	20.1	39.5	25.6	22.0
20	11.9	26.8	21.5	14.2

broad distribution and many large crystallites, the M-500 is intermediate between this and the L-500.

Let us now examine the exposed surface of the crystallites as measured by hydrogen chemisorption. Figure 8 shows typical adsorption isotherms for a series of sintering times. As discussed earlier, extrapolation according to Eq. (1) gives the surface of the crystallites. Table 8 shows these results for each of the samples.

Measured surface areas are consistently lower than those calculated from crystallite size distributions. Desai and Richardson interpreted this phenomena as "inacessibility" in which only a fraction of the surface is available for hydrogen chemisorption due to either interaction with the support or to plugging of pores (*20*). Values of the accessibility factor, α, defined as the ratio between measured and calculated nickel surface areas, are given in Table 9.

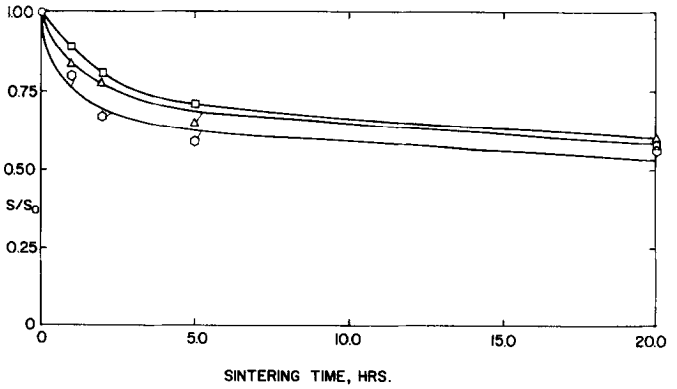

FIG. 6. Surface area loss and calculated decay curves. (□) L-500, (△) M-500, (○) H-500.

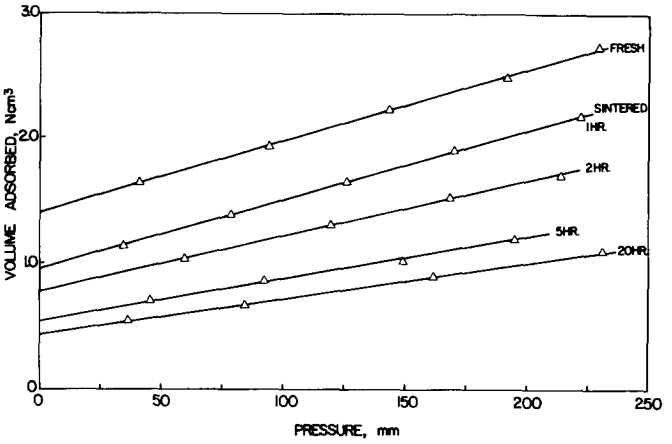

FIG. 7. Hydrogen chemisorption isotherms for M-600.

Absolute values of accessibility factors depend upon the assumed spherical crystallite shape, but trends are the same if this is not true. Two conclusions emerge. First, all cases show a decrease on sintering, indicating that as the crystallites grow further obstruction results from filling the pore. For example, sintering L-500 shows a drop in α from 0.241 to 0.085 in 20 h. The crystallite radius has increased from 2.25 to 3.23 nm, approaching the pore radius of 4.11 nm. The distribution is also broader so that a large fraction of the crystallites are now "wedged" into the pores and the metal surface area is more physically blocked.

Increasing the pore radius in M-500 results in a larger value of α, more accessible surface and less blockage. However, there is a decrease in α for H-500, with larger pores, but it should be remembered that this support shows considerable pore mouth constriction. Presumably, increased blockage is responsible for lower α values.

Since the values of M_∞ do not change on sintering, inaccessibility must be a physical rather than electronic effect, i.e., surface blockage and not so-called strong metal–support interactions.

TABLE 9

Loss of Accessible Surface

Sintering time (h)	Accessibility factor, α			
	L-500	M-500	H-500	M-600
0	0.241	0.434	0.351	0.460
1	0.188	0.327	0.299	0.233
2	0.133	0.287	0.237	0.174
5	0.118	0.242	0.187	0.175
20	0.085	0.181	0.163	0.119

CONCLUSIONS

These experiments show that when all other factors are held constant, sintering rates are decreased when the pore size approaches the size of the crystallite. The pore size distribution influences the final or "stable" crystallite size distribution. Although narrow pores decrease sintering rates, the effect is more than offset by a decrease in accessibility. Growing crystallites fill the pores and the crystallite surface becomes increasingly blocked.

These features should be considered when theories for sintering of crystallites in porous supports are attempted.

ACKNOWLEDGMENT

We are grateful to the National Science Foundation for support of this research under Grant ENG76-10071.

REFERENCES

1. Van Hardeveld, R., and Hartog, F., "Advances in Catalysis," Vol. 22, p. 75. Academic Press, New York, 1972.

2. Lee, H. H., and Ruckenstein, E., *Catal. Rev. Sci. Eng.* **25,** 475 (1983).
3. Flynn, P. C., and Wanke, S. E., *J. Catal.* **34,** 300 (1974).
4. Flynn, P. C., and Wanke, S. E., *J. Catal.* **34,** 390 (1974).
5. Flynn, P. C., and Wanke, S. E., *J. Catal.* **37,** 432 (1974).
6. Wanke, S. E., and Flynn, P. C., *Catal. Rev.* **12,** 93 (1975).
7. Geus, J. W., *in* "Chemisorption and Reactions on Metallic Films" (J. R. Anderson, Ed.). Academic Press, New York, 1971.
8. Bett, J. A., Kinoshita, R., and Stonehart, P., *J. Catal.* **35,** 307 (1974).
9. Ruckenstein, E., and Dadyburjes, D. B., *Thin Solid Films* **55,** 89 (1978).
10. Ruckenstein, E., and Pulvermacher, B., *AIChE J.* **19,** 356 (1973).
11. Ruckenstein, E., and Pulvermacher, B., *J. Catal.* **29,** 224 (1973).
12. Ruckenstein, E., and Pulvermacher, B., *J. Catal.* **35,** 115 (1974).
13. Wynblatt, P., and Gjostein, N. A., *Prog. Solid State Chem.* **9,** 21 (1973).
14. Granquist, C. G., and Buhrman, P. A., *J. Appl. Phys.* **27,** 693 (1975).
15. Granquist, C. G., and Buhrman, P. A., *Solid State Commun.* **17,** 123 (1976).
16. Granquist, C. G., and Buhrman, P. A., *J. Appl. Phys.* **47,** 2200 (1976).
17. Granquist, C. G., and Buhrman, P. A., *J. Catal.* **46,** 238 (1977).
18. Wanke, S. E., *J. Catal.* **46,** 234 (1977).
19. Wynblatt, P., and Ahn, T. M., *in* "Sintering and Catalysis" (G. C. Kuczinski, Ed.). Plenum, New York, 1975.
20. Desai, P. H., and Richardson, J. T., "Catalyst Deactivation." Elsevier, Amsterdam, 1980.
21. Lee, H. H., *J. Catal.* **63,** 129 (1980).
22. Pask, J. A., and Fulrath, R. M., *J. Amer. Ceram. Soc.* **45,** 592 (1962).
23. Bartholomew, C. H., Pannell, R. B., and Fowler, R. W., *J. Catal.* **79,** 34 (1983).
24. Bartholomew, C. H., and Sorensen, W. L., *J. Catal.* **81,** 131 (1983).
25. Williams, A., Butler, G. A., and Hammonds, J., *J. Catal.* **24,** 352 (1972).
26. Kuo, H. K., and De Angelis, R. J., *J. Catal.* **68,** 203 (1981).
27. Ruckenstein, E., and Pulvermacher, B., *J. Catal.* **37,** 416 (1975).
28. Mills, G. A., and Steffgen, F. W., *Catal. Rev.* **8,** 159 (1973).
29. Vannice, M. A., *Catal. Rev.* **14,** 153 (1976).
30. Cale, T. S., and Richardson, J. T., *J. Catal.* **79,** 378 (1983).
31. Richardson, J. T., and Crump, J. G., *J. Catal.* **57,** 417 (1979).
32. Richardson, J. T., Crump, J. R., and Osterwalder, R. U., *in* "Sintering and Catalysis" (G. C. Kuczinski, Ed.). Plenum, New York, 1979.
33. Leclous, A. J., *in* "Catalysis, Science and Technology, Vol. 2" (J. R. Anderson and M. Boudart, Eds.). Springer-Verlag, New York, 1981.
34. Van Dillen, J. A., Geus, J. W., Hermans, L. A. M., and van der Meijden, J., *in* "Proceedings, 6th International Congress on Catalysis, London, 1976" (G. C. Bond, P. B. Wells, and F. C. Tomkins, Eds.). The Chemical Society, London, 1976.
35. Richardson, J. T., and Dubus, R. J., *J. Catal.* **54,** 207 (1978).
36. Coenen, J. W. G., and Linsen, B. F., "Physical and Chemical Aspects of Adsorbents and Catalysts." Academic Press, New York, 1970.
37. Richardson, J. T., and Cale, T. S., submitted for publication.